Effect of roughness on the adhesive tractions between contacting bodies

Junki Joe[a,*], M.D. Thouless[a], J. R. Barber[a]

[a]*Department of Mechanical Engineering,University of Michigan, Ann Arbor, MI 48109-2125, U.S.A.*

Abstract

A method is proposed for estimating the effect of broad spectrum surface roughness on the adhesion between elastic bodies. At each length scale, the effect of fine scale roughness is modelled by a modified traction law whilst an added coarse scale increment is described by a probability distribution of mean gap as modified by elastic deformation. Instabilities occur for relatively smooth surfaces whose linear dimensions are sufficiently large to support long wavelength perturbations. The method is validated by comparison with direct numerical calculations, in the range where this is practicable. It is then applied to power-law spectra with various values of height variance and lower wavenumber cutoff. The results show that the effect of roughness is dominated by the height variance m_0, but at lower wavenumber elastic deformation reduces the dependence on m_0, except near the unstable range.

Keywords: Contact mechanics; surface roughness; adhesion.

1. Introduction

If the surfaces of two contacting bodies were perfectly smooth and plane, the tractions between them would be determined by a potential law characterizing the physics of the intermolecular forces, and in particular would exhibit a range of separations in which these tractions would be attractive. However, the inevitable presence of surface roughness weakens the adhesive tractions. Indeed, Fuller and Tabor [1] showed that even minor roughness can seriously degrade the adhesion between contacting bodies.

*Corresponding author: jkjoe@umich.edu.

Many researchers have developed models to predict the effect of surface roughness on contact. Since contact is expected to be concentrated near the highest points of the two surfaces, many of these theories depend on approximating the rough surface profile by a distribution of asperities, which are then assumed to act independently. Greenwood and Williamson [2] showed that the behaviour predicted by such a model is largely determined by the height and local curvature distribution of the asperities and considerable effort has been expended in extracting this information from surface profile measurements [3]. However, high resolution measurements of surface profiles show that roughness exhibits multiscale features over several decades of length scale [4]. This implies that if an asperity is defined as a point higher than its nearest neighbours, the asperity parameters and some of the predictions of the resulting model are sensitive to the resolution of the surface measuring instrument.

An alternative approach, pioneered by Persson [5], is to characterize the rough surface contact problem by the probability distribution function [PDF] $\Phi(p,k)$ for the contact pressure p at a random point, when the power spectral density [PSD] $P(k)$ of the surface roughness is truncated at some wavenumber k. The modification of $\Phi(p)$ due to the introduction of a small increment $(k, k+\Delta k)$ of the PSD is then estimated. The PDF $\Phi(p)$ due to the entire PSD can then be determined by iteration or integration. This technique was introduced earlier by Ciavarella *et al.* to investigate the contact of a surface defined by the Weierstrass profile [6].

In a previous paper [7], we introduced a modification to Persson's theory in which we (i) tracked the PDF $\Phi(g)$ for the local separation [gap] g between the surfaces rather than the contact pressure, and (ii) determined the effect of an infinitesimal increment in the PSD using a linear perturbation of the traction law between plane surfaces [8] about the local value of g. The reason for developing this theory in terms of g was that the local traction $\sigma_0[=-p]$ is always a unique function of g, whereas if a tensile range $[\sigma_0 > 0]$ exists, g is not a unique function of σ_0. This is illustrated for the Lennard-Jones traction law in Figure 1, but it is clearly the case for any traction law, including those we shall use in the following analysis for the mean traction between rough surfaces.

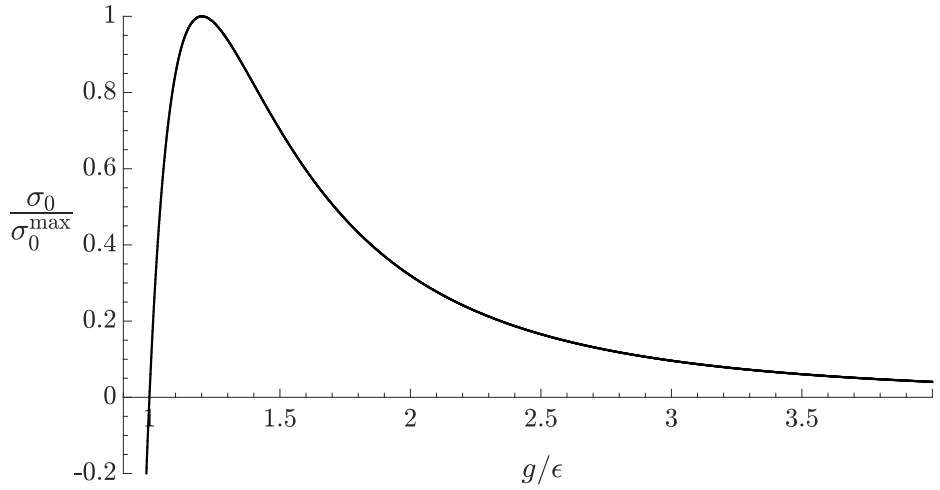

Figure 1: The Lennard-Jones interface traction law. The separation g is normalized by the equilibrium spacing ϵ between the surfaces.

The method described in [7] gives predictions of the relation between the mean traction $\bar{\sigma}$ and mean gap $\bar{g}$ that agree closely with direct numerical simulations for cases where the roughness PSD is restricted to high wavenumbers k. However, it cannot be extended to a broader spectrum because the incremental problem is unstable for wavenumbers that are low enough for the maximum negative slope of the traction law to exceed the positive stiffness of the contacting bodies subjected to a spatially sinusoidal traction. This is a real physical effect. Ghatak *et al.*[9, 10] have shown experimentally that for thin elastic films, nominally uniform contact can bifurcate into regular patterns. An energetic analysis of this phenomenon [11, 12] predicts instabilities for layers of any thickness, including the half space, if the wavelength is sufficiently large [i.e. k sufficiently small]. An arbitrarily small perturbation of the given wavenumber [i.e. any non-zero content in the PSD in that range] is then sufficient to trigger the instability.

In this context we should note that practical contact problems necessarily involve bodies of finite dimensions, and the description of the surface in terms of a PSD [and particularly a power-law PSD] is then meaningful only for wavelengths much smaller than the linear dimensions of the macroscopic contact area. Practical surfaces are likely to exhibit stochastic and/or deterministic deviations from the plane outside this range, and these can also be expected to influence the contact morphology and hence the adhesive force

law.

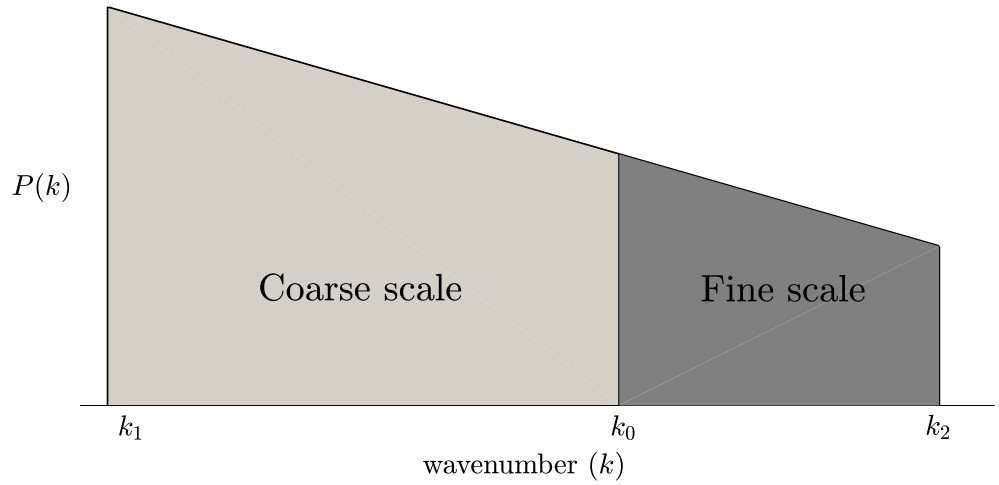

Figure 2: Partition of the power spectral density [PSD] into 'fine scale' and 'coarse scale' components.

In the present paper, we shall overcome this difficulty by applying the technique from [7] sequentially. To illustrate the concept, Figure 2 shows a representative PSD in the range $k_1 < k < k_2$ which has been arbitrarily separated into coarse-scale $[k_1 < k < k_0]$ and fine-scale $[k_0 < k < k_2]$ components. Suppose that k_0 is sufficiently large to permit the method of reference [7] to be used to determine the relation $\bar{\sigma}(\bar{g})$ for a plane surface containing *only* the fine scale roughness. We can then consider the entire PSD of Figure 2 as defining a surface whose PSD contains only the coarse scale roughness, but for which the interface traction law is $\bar{\sigma}(\bar{g})$ rather than $\sigma(g)$. In other words, at this stage, the coarse scale is modelled explicitly, but the effect of the fine scale is reflected in a modified traction law. Since $\bar{\sigma}(\bar{g})$ will generally have a lower maximum negative slope than $\sigma(g)$ [the fine-scale roughness attenuates the attractive tractions], this allows us to proceed to lower wavenumbers without encountering an instability in the incremental problem.

2. Theory

If the force between two molecules is assumed to follow the Lennard-Jones 6-12 law, the traction $\sigma_0(g)$ between two bodies bounded by plane surfaces

and separated by a distance g is given by

$$\sigma_0(g) = \frac{8\Delta\gamma_0}{3\epsilon}\left(\frac{\epsilon^3}{g^3} - \frac{\epsilon^9}{g^9}\right) , \tag{1}$$

[8], where $\Delta\gamma_0$ is the interface energy per unit area and ϵ is the equilibrium spacing. The maximum tensile traction then occurs at $g = 3^{1/6}\epsilon \approx 1.201\epsilon$ and is

$$\sigma_0^{\max} = \frac{16\Delta\gamma_0}{9\sqrt{3}\epsilon} . \tag{2}$$

We shall use these results in the following derivations, but we note that the same method can be applied to any other traction law for which the function $\sigma_0(g)$ is known or assumed.

2.1. Probability function for gap

Suppose that a rough surface is placed near to a plane surface such that the mean gap is g, and that, in this configuration, the probability of a given point having a local gap s is $\Phi(s|g)$. The mean traction $\sigma(g)$ between the surfaces can then be found by convolution with the traction law as

$$\sigma(g) = \int_0^\infty \Phi(s|g)\sigma_0(s)ds . \tag{3}$$

We shall refer to $\sigma(g)$ as the *effective traction law* for a surface of the given roughness. It corresponds to the traction law that would be measured experimentally for nominally plane but actually slightly rough surfaces.

We next extend the definition of the conditional PDF such that $\Phi(s|g;k_1,k_2)$ denotes the conditional probability $\Phi(s|g)$ for the case where the roughness is defined by that part of a given PSD $P(k)$ in the range $k_1 < k < k_2$. If $P(k)$ is partitioned into two ranges as in Figure 2, it then follows that

$$\Phi(s|g;k_1,k_2) = \int_0^\infty \Phi(s|t;k_0,k_2)\Phi(t|g;k_1,k_0)dt , \tag{4}$$

since points that are separated by t for the PSD (k_1,k_0) will be distributed by the conditional probability $\Phi(s|t;k_0,k_2)$ when the roughness spectrum (k_0,k_2) is added.

If we now apply the operator (3) to both sides of equation (4), we obtain

$$\begin{aligned}\sigma(g;k_1,k_2) &= \int_0^\infty\int_0^\infty \Phi(s|t;k_0,k_2)\Phi(t|g;k_1,k_0)\sigma_0(s)dtds \\ &= \int_0^\infty \Phi(t|g;k_1,k_0)\sigma(t;k_0,k_2)dt \end{aligned} \tag{5}$$

after changing the order of integration, where

$$\sigma(t; k_0, k_2) = \int_0^\infty \Phi(s|t; k_0, k_2)\sigma_0(s)ds \tag{6}$$

is the effective traction law for a surface containing only the roughness in (k_0, k_2).

Clearly this argument can be applied sequentially to a PSD partitioned into any number N of tranches. At each stage, the effective traction law determined up to that point is used in place of $\sigma_0(g)$ to determine the new traction law when the next tranche is included.

2.2. Conditional probability

An essential stage in the procedure is the determination of the conditional probability distribution $\Phi(s|g)$ given the PSD $P(k)$ when $k \in (k_{i-1}, k_i)$ and the most recent effective traction law $\sigma_i(g) = \sigma(g; k_i, k_N)$. If the added roughness is sufficiently small, this problem can be solved as in [7], but using a local linear perturbation of the non-linear function $\sigma_i(g)$, in combination with the elastic solution for a half-space[1] loaded by a prescribed sinusoidal traction.

The derivations are given in [7] and are omitted here in the interests of brevity. We obtain

$$\Phi(t|g; k_{i-1}, k_i) = \frac{1}{\sqrt{2\pi V}} \exp\left(-\frac{(t-g)^2}{2V}\right) , \tag{7}$$

where the variance

$$V = 2\pi \int_{k_{i-1}}^{k_i} kP(k) \left[1 + \frac{2}{E^* k}\frac{\partial \sigma_i}{\partial g}\right]^{-2} dk , \tag{8}$$

$$\frac{1}{E^*} = \frac{(1-\nu_1^2)}{E_1} + \frac{(1-\nu_2^2)}{E_2} , \tag{9}$$

and E_j, ν_j, $j = 1, 2$ are the Young's modulus and Poisson's ratio respectively for body j. These results reduce to equations (14–17) of [7] if $\sigma_i(g)$ is replaced by the Lennard-Jones law $\sigma_0(g)$ of equation (1).

[1]Notice that the method described here is easily generalized to the problem of a thin elastic layer by replacing the elastic term in equation (8) by the solution corresponding to sinusoidal loading of the layer.

3. Numerical solution and convergence

The procedure described above [and in particular equations (7, 8)] depends on a linearization of $\sigma_i(t)$ about $t = g$, which should be a good approximation provided that

$$V\frac{\partial^2\sigma_i}{\partial g^2} \ll \left[\frac{\partial\sigma_i}{\partial g} + \frac{E^*k}{2}\right] . \tag{10}$$

This in turn requires that the intervals (k_{i-1}, k_i) be sufficiently small, and that appropriate values can be chosen based on a conventional convergence study. However, the condition (10) suggests that larger intervals can be used at smaller values of k to increase computational efficiency. Numerical experiments with several different PSDs showed that converged results can be obtained by choosing k_{i-1} such that

$$\mathcal{E}(g) \equiv \frac{2m_0(\Delta k)}{E^*k_i}\left|\frac{\partial^2\sigma_i}{\partial g^2}\right|\left[1 + \frac{2}{E^*k_i}\frac{\partial\sigma_i}{\partial g}\right]^{-3} < 2\times 10^{-5} \tag{11}$$

for all g, where

$$m_0(\Delta k) = 2\pi\int_{k_{i-1}}^{k_i} kP(k)dk \tag{12}$$

is the height variance associated with the tranche $\Delta k = (k_{i-1}, k_i)$ of the PSD. If the PSD $P(k)$ has power-law form corresponding to a fractal dimension D, the criterion (11) defines a set of values k_i which are approximately proportional to i^λ at small wave numbers, with $\lambda \approx 7 - 2D$.

3.1. Comparison with direct numerical computations

The strength of the present method is that it can be used for broadband spectra where the ratio of upper to lower wavenumber k_N/k_1 is relatively large. Direct numerical solutions [e.g. boundary-element or finite-element studies] are limited to values of this ratio of the order of 100. Furthermore, they can only give results for particular random realizations of the underlying statistics, requiring multiple calculations to yield appropriate averages. However, as a check on the present procedure, we compared our results with numerical solutions using the 'Green's function molecular dynamics' [GFMD] code developed by Persson and Scaraggi [13] for a PSD of power-law form

with a fractal dimension $D = 2.2$, $\tilde{k}_1 = 0.8, \tilde{k}_2 = 8.0$ and height variace $m_0 = 0.66\epsilon^2$, where the dimensionless wavenumber is defined by

$$\tilde{k} = \chi k \quad \text{with} \quad \chi = \frac{3\epsilon^2 E^*}{16\Delta\gamma_0} \,. \tag{13}$$

Figure 3 shows the predicted relation between the normalized mean interface traction $\sigma/\sigma_0^{\max}$ and gap g/ϵ [solid black line] and numerical simulations using several realizations of the same PSD [thin red lines]. The present prediction lies well within the variance of these realizations, except in a range very close to the equilibrium gap, where the theoretical line is lower than the mean of the simulations.

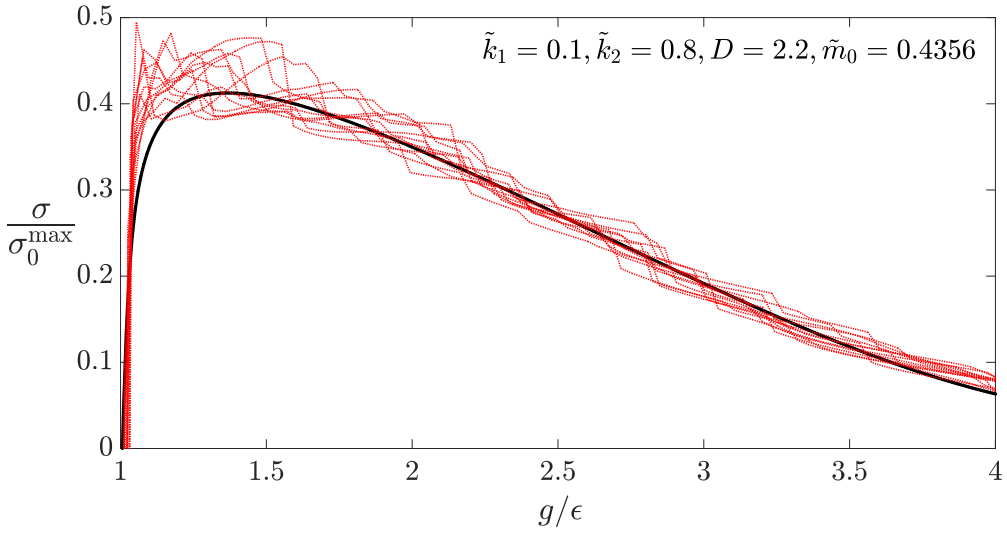

Figure 3: Traction law $\sigma(g)$ for contact between a nominally plane rough surface and a flat. The roughness spectrum is a power-law with fractal dimension $D = 2.2$, dimensionless wavenumbers $0.8 < \tilde{k} < 8.0$ and height variance $m_0 = 0.4356\epsilon^2$. The solid line represents the predictions of the present theory and the thin red lines represent numerical solutions using the 'GFMD' code from [13].

For practical applications, interest is focussed mainly on the effective interface strength $\sigma^{\max}$ [the maximum value of the traction in Figure 3] and the effective interface energy $\Delta\gamma_{\text{eff}}$ [the area underneath the curve in Figure 3]. This latter term is the work per unit area needed to separate the rough

surfaces from the equilibrium separation. The analytical predictions for these quantities using the present theory are $\sigma^{\max} = 0.41\sigma_0^{\max}$ and $\Delta\gamma_{\rm eff} = 0.88\Delta\gamma_0$, whereas a curve $\sigma(g)$ averaged over those from 12 numerical realizations gives $\sigma^{\max} = 0.43\sigma_0^{\max}$ and $\Delta\gamma_{\rm eff} = 0.89\Delta\gamma_0$ respectively.

As a further check, Figure 4 compares our predictions for the pull-off traction $\sigma^{\max}$ for the somewhat broader PSD defined by Figure 18 of [13] with numerical [GFMD] calculations and theoretical predictions both taken from Figures 15 and 17 of the same paper, for four different values of the interface energy $\Delta\gamma$ for plane surfaces. The agreement between the present theory and the GFMD calculations is clearly very satisfactory.

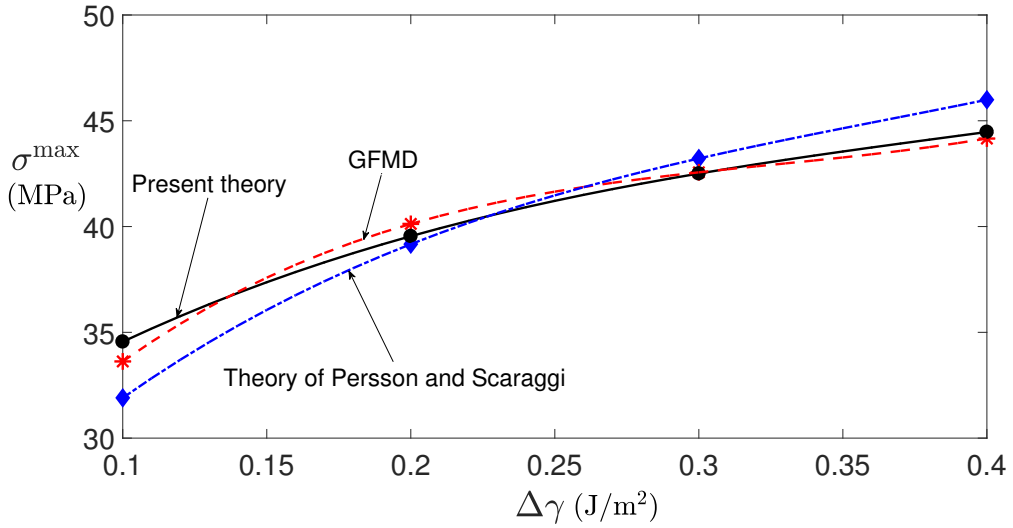

Figure 4: The solid line shows the predicted pull-off traction $\sigma^{\max}$ for the PSD defined by Figure 18 of [13], which has fractal form with $D = 2.2$ in the range $k_r < k < 8k_r$ and is constant in $k_r/4 < k < k_r$, where the roll-off wavenumber $k_r = 10^6$ m^{-1}. The RMS roughness height is $h_{\rm RMS} = 0.52$ nm. Theoretical predictions [dotted line] and numerical [GFMD] calculations [dashed line] from [13] are shown for comparison. [This figure is plotted with dimensional axes to facilitate comparison with [13]].

4. Results

The comparisons in Section 3.1 show that the proposed solution gives good predictions of the effect of surface roughness on adhesive traction parameters, so we now apply the method to broader roughness spectra, for

which direct numerical calculations would be very computationally intensive. In the interests of generality, we present the results in terms of the dimensionless wavenumber $\tilde{k}$ of equation (13).

We restrict attention to power-law PSDs, which can be characterized by the lower and upper dimensionless wavenumbers $\tilde{k}_1$ and $\tilde{k}_2$, the fractal dimension D and the dimensionless height variance

$$\widetilde{m}_0 = \frac{m_0}{\epsilon^2} = \left(\frac{h_{\mathrm{RMS}}}{\epsilon}\right)^2 . \tag{14}$$

Figure 5 shows the effect of height variance on $\sigma^{\max}$ and $\Delta\gamma_{\mathrm{eff}}$, for a fractal PSD with $\tilde{k}_1 = 0.04, \tilde{k}_2 = 8$ and $D = 2.2$. In this range, $\widetilde{m}_0$ has a dramatic effect on both these measures of adhesion. Changing $\widetilde{m}_0$ by a factor of 200 [from 0.5 to 100 and hence h_{RMS} from 0.7ϵ to 10ϵ] reduces $\Delta\gamma_{\mathrm{eff}}$ by a factor of 1,000 and $\sigma^{\max}$ by a factor of 25,000.

The dashed line in Figure 5 represents the analytical prediction for $\sigma^{\max}$ defined by Ciavarella [14] based on a 'Bearing Area' approximation to the adhesive tractions. This method underestimates $\sigma^{\max}$ [perhaps because of the empirical factor in the bearing area calculation], but tracks the shape of the curve well except at larger values of $\widetilde{m}_0$.

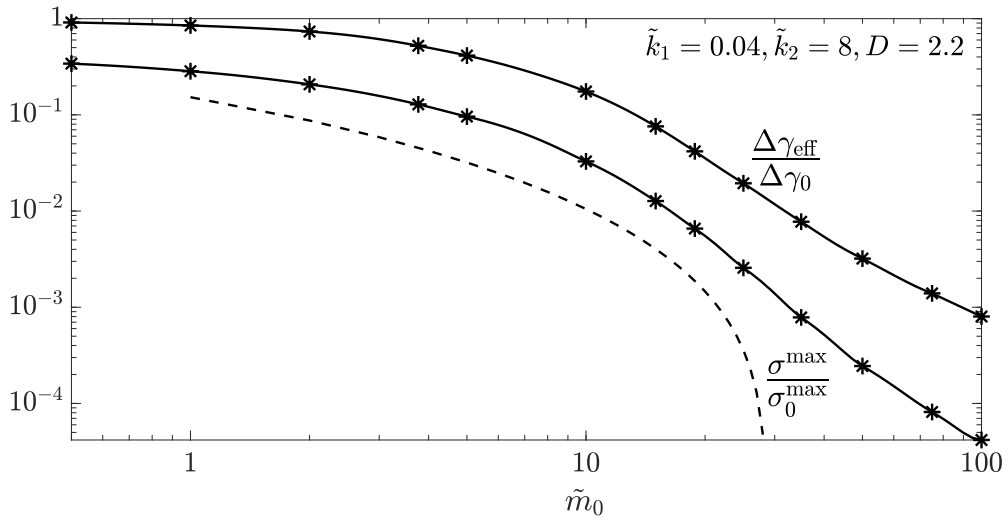

Figure 5: The effect of dimensionless height variance $\widetilde{m}_0$ on $\sigma^{\max}$ and $\Delta\gamma_{\mathrm{eff}}$ for fractal roughness with $D = 2.2$ and $\tilde{k}_1 = 0.04, \tilde{k}_2 = 8$. The dashed line

shows the corresponding prediction of Ciavarella's 'Bearing Area Method' [14] for $\sigma^{\max}$.

We showed in [7] that the gap distribution $\Phi(g)$ and hence the effective traction law $\sigma(g)$ for a fractal surface converge as the upper cutoff $\tilde{k}_2 \to \infty$, since eventually the amplitudes of any added waves are small compared with the length scale of the intrinsic force between the surfaces. Results from the present analysis confirm that changing $\tilde{k}_2$ has relatively little effect on $\sigma^{\max}$ and $\Delta\gamma_{\text{eff}}$ once it approaches a practical limit of the atomic scale. By contrast, the lower cutoff $\tilde{k}_1$ has a significant effect, as shown in Figure 6, which plots these quantities as functions of $\tilde{k}_1$ for fixed values of $\widetilde{m}_0, \tilde{k}_2$ and D.

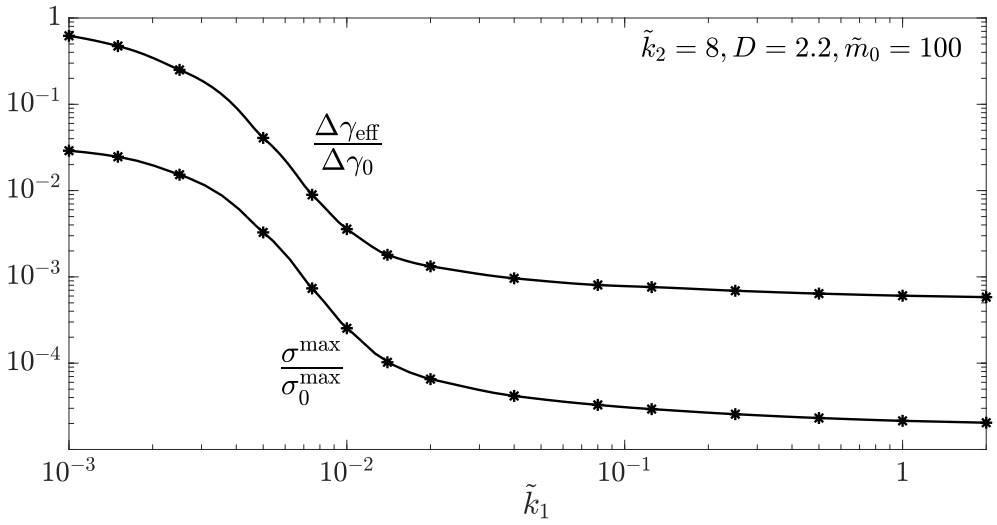

Figure 6: The effect of lower cutoff $\tilde{k}_1$ on $\sigma^{\max}$ and $\Delta\gamma_{\text{eff}}$ for fractal roughness with $\tilde{k}_2 = 8, \widetilde{m}_0 = 100$ and $D = 2.2$.

This result has a simple physical explanation. The amplitude of the traction distribution needed to flatten a single sine wave elastically is proportional to the surface slope, so the short wavelength roughness is very difficult to deform. The behaviour in this range is dominated by the interfacial traction law and the height distribution, and is therefore well characterized by m_0. This is the range described by Persson and Scaraggi [13] as the 'DMT-limit'. However, at lower wavenumbers, elastic deformation becomes increasingly dominant, and the effect of coarse scale roughness tends to that predicted

using a hard contact theory. We also note that for a given roughness profile, a reduction in elastic modulus reduces χ in equation (13). This in turn reduces $\tilde{k}_1$ and hence leads to increased values of $\sigma_{\max}$ and $\Delta\gamma_{\text{eff}}$ [i.e. enhanced adhesion], as shown in Figure 6. Of course $\tilde{k}_2$ will also be reduced but we have already shown that the results are insensitive to this parameter provided it is sufficiently large.

4.1. Effect of fractal dimension

All the results presented above are for a surface PSD with fractal dimension $D = 2.2$. Reducing D for given values of the other parameters has the effect of moving contributions from the variance $\widetilde{m}_0$ towards lower wavenumbers, where we have already seen the effect of roughness on both $\sigma^{\max}$ and $\Delta\gamma_{\text{eff}}$ is somewhat reduced. This tendency is confirmed by Figure 7, for $\tilde{k}_1 = 0.05, \tilde{k}_1 = 8, \widetilde{m}_0 = 0.4356$. However, the effect is relatively modest, implying that the results for $D = 2.2$ should be reasonably representative for other practical fractal dimensions.

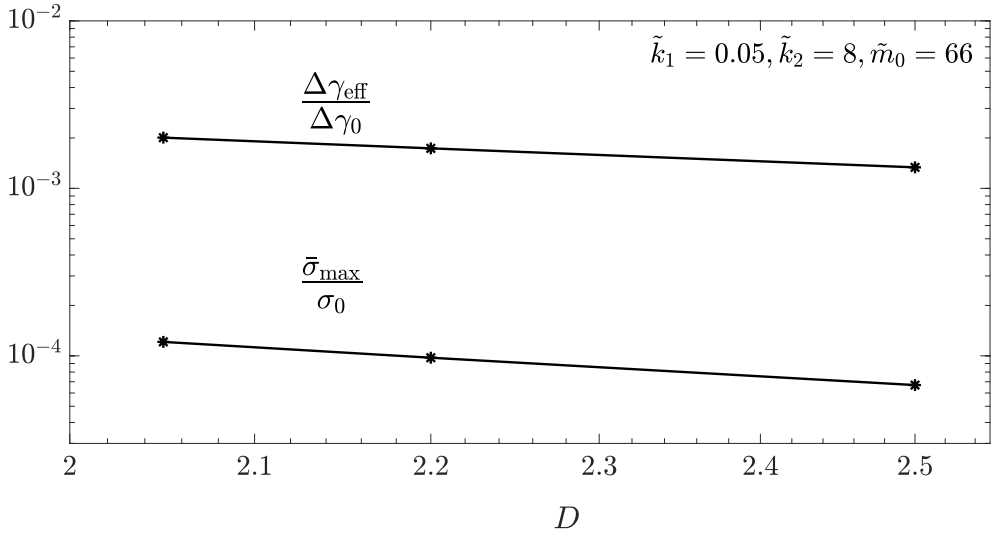

Figure 7: The effect of fractal dimension D on $\sigma^{\max}$ and $\Delta\gamma_{\text{eff}}$ for fractal roughness with $\tilde{k}_1 = 0.05, \tilde{k}_2 = 8$ and $\widetilde{m}_0 = 66$.

4.2. Contour plot

Each point in Figures 5 and 6 involves the calculation of the effective traction law $\sigma_i(g)$ for the PSD truncated at at a progressively lower wavenumber

cutoff k_i and therefore provides implicit information about the pull-off traction $\sigma^{\max}$ and the effective interface energy $\Delta\gamma_{\text{eff}}$ at a series of points along a line in (m_0, k_1)-space. These data were used to construct the contour plots of Figure 8 [for $\sigma^{\max}$] and Figure 9 [for$\Delta\gamma_{\text{eff}}$] for power-law PSDs with $\tilde{k}_2 = 8$ and $D = 2.2$.

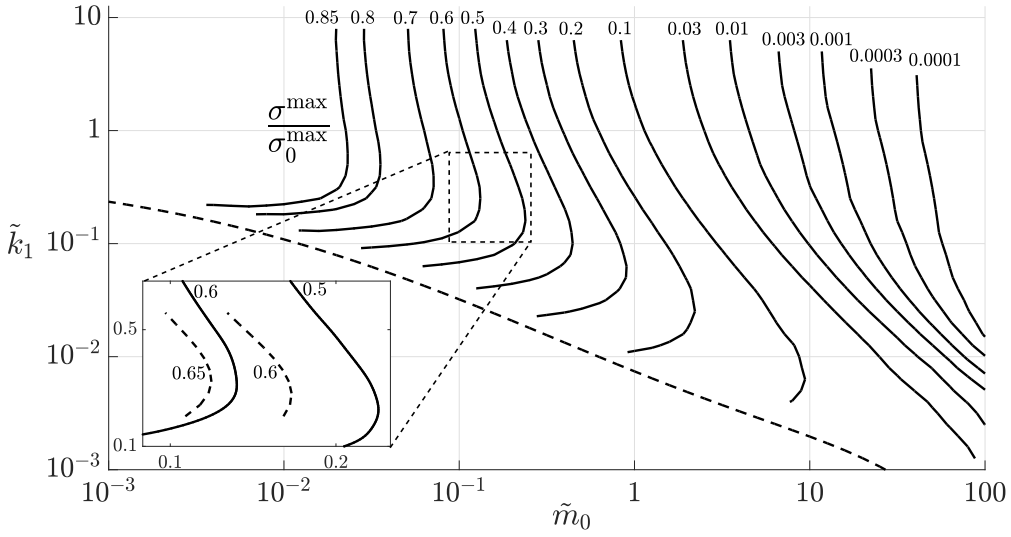

Figure 8: Contour plot of normalized pull-off traction $\sigma^{\max}/\sigma_0^{\max}$ as a function of $\tilde{k}_1, \widetilde{m}_0$ for fractal roughness with $\tilde{k}_2 = 8$ and $D = 2.2$. The inset compares contours in the dashed rectangle from the present theory [solid lines] with those from the GFMD code [dashed lines] using a single realization for each point.

The bottom left region of each of these figures [below the dashed line] defines parameter values in which the reduction of maximum negative slope in the effective traction law $\bar{\sigma}(\bar{g})$ due to surface roughness is insufficient to prevent instability. In this range, if the linear dimensions of the surface are sufficiently large to support a sine wave of the given value of $\tilde{k}_1$, we can anticipate periodic structures of the type documented by Chaudhury and Shenoy [9, 10, 11, 12], even if the roughness PSD contains no waves of this wavelength.

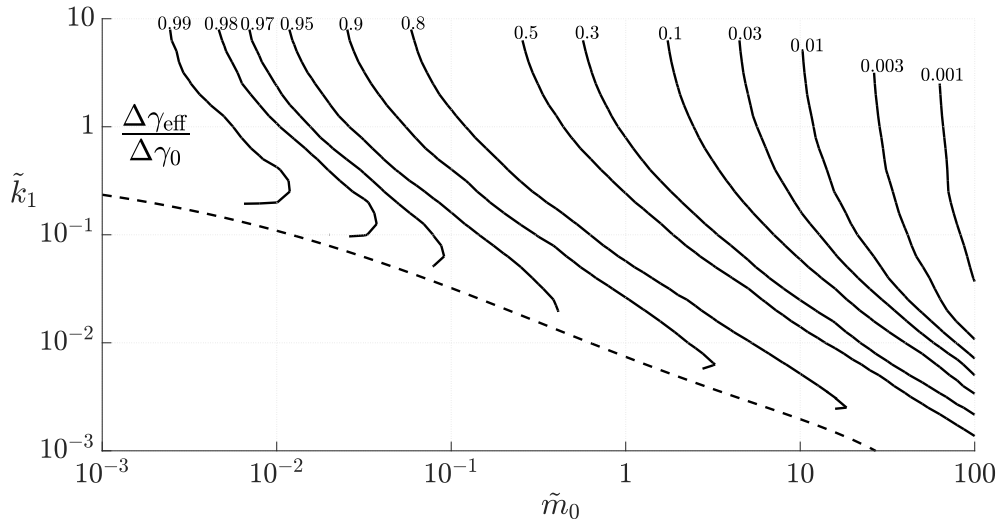

Figure 9: Contour plot of normalized effective interface energy $\Delta\gamma_{\text{eff}}/\Delta\gamma_0$ as a function of $\tilde{k}_1, \widetilde{m}_0$ for fractal roughness with $\tilde{k}_2 = 8$ and $D = 2.2$.One

consequence of these instabilities is that there then exist two stable equilibrium states for a given value of mean separation, so that the loading and unloading curves will generally be different. This implies hysteretic energy loss during a loading/unloading cycle, and since different regions encounter the instability at different points in the loading cycle, the unloading cycle and the hysteretic loss will depend on the maximum compressive traction during loading. Results of this kind have been documented in asperity models[15] and in numerical models [16]. One method of quantifying these effects would be to use a partition of the PSD as shown schematically in Figure 2, such that inclusion of the fine scale alone defines a point in the stable range in Figures 8,9 and hence leads to a single-valued traction law. This law could then be used in a numerical solution of the coarse-scale problem. This is a subject of ongoing research.

The contours in these figures start to curve backwards as the unstable region is approached, particularly for the pull-off traction $\sigma^{\max}$ in Figure 8. This implies a greater reduction of adhesion in this region as k_1 is reduced. Physically this arises because long wavelength sinusoids experience relatively large amplitudes of elastic deformation, which increase the variance of the local gap g in regions where the traction law has a negative slope. In effect, the PDF $\Phi(g)$ is already starting to develop the bimodal form associated with the unstable patterns described in [9, 10, 11, 12].

To ensure that these results were not the result of a fictitious numerical instability, we ran numerical [GFMD] examples in the range defined by the dotted rectangle in Figure 8. In this range, numerical calculations are computer-intensive but not prohibitively so. Since each run of the GFMD code defines only one realization of the underlying statistics, a precise check on the theory is not possible, but the predicted pull-off traction for all the cases analyzed were within $\pm 10\%$ of the predicted values. More importantly, the GFMD results confirm that the pull-off traction falls with decreasing k_1 near the stability boundary, implying that the contours have the shape shown in Figure 8.

5. Conclusions

The paper presents an efficient procedure for predicting the effect of broad sprectrum surface roughness on the effective adhesive traction law — i.e. the relation between nominal adhesive traction and mean gap. Results agree well with the averages of direct numerical simulations for the relatively narrower spectra over which such simulations are computationally practicable.

Contour plots are presented for the nominal pull-off traction and effective interface energy for broader power-law spectra as a function of lower cutoff wavenumber and height variance. The calculations show that instabilities occur for relatively smooth surfaces whose linear dimensions are sufficiently large to support long wavelength perturbations. This is a physical effect that has been documented both experimentally and theoretically. Near the unstable range, a greater reduction in adhesive effects is predicted and this behaviour has been confirmed for relatively narrow spectra using numerical simulations.

At large wavenumbers [short wavelengths], the effect of roughness on adhesion is well-characterized by the height variance m_0, but at lower wavenumbers elastic effects become more important and incremental contributions to m_0 have less effect, except near the unstable range.

References

[1] Fuller KNG, Tabor D. The effect of surface roughness on the adhesion of elastic solids. Proc R Soc Lond 1975;A345:327–342.
doi: 10.1098/rspa.1975.0138

[2] Greenwood JA, Williamson JBP. The contact of nominally flat surfaces. Proc R Soc Lond 1966;A295:300–319. doi: 10.1098/rspa.1966.0242

[3] Nayak PR.Random process model of rough surfaces, ASME J Lub Tech 1971;93(3):98–407. doi: 10.1115/1.3451608

[4] B. B. Mandelbrot, D. E. Passoja, A. J. Paullay, Fractal character of fracture surfaces of metals, Nature308 (5961) (1984) 721–722.

[5] Persson BNJ. Theory of rubber friction and contact mechanics. J Chem Phys 2001;115:3840–3861. doi: 10.1063/1.1388626

[6] Ciavarella M, Demelio G, Barber JR, Jang YH. Linear elastic contact of the Weierstrass profile. Proc R Soc Lond 2000;A456:387–405. doi: 10.1098/rspa.2000.0522

[7] J. Joe, M. Scaraggi, J. Barber, Effect of fine-scale roughness on the tractions between contacting bodies,Tribology International 111 (2017) 5256.

[8] D. Maugis, *Contact, Adhesion and Rupture of Elastic Solids*, Springer, New York (2000).

[9] Ghatak A, Chaudhury MK, Shenoy V, Sharma A, Meniscus instability in a thin elastic film Phys. Rev. Lett 2000;85(20):4329–4332.

[10] Ghatak A, Chaudhury MK, Adhesion-induced instability patterns in thin confined elastic film Langmuir 2003; 19: 2621–2631.

[11] J. Sarkar, V. Shenoy, A. Sharma. Patterns, forces, and metastable pathways in debonding of elastic films. Phys. Rev. Lett 2004; 93 (1) 018302. doi: 10.1103/PhysRevLett.93.018302

[12] J. Sarkar, A. Sharma, V. Shenoy. Adhesion and debonding of soft elastic films: Crack patterns, metastable pathways, and forces. Langmuir 2005; 21: 1457–1469.

[13] Persson BNJ, Scaraggi M. Theory of adhesion: Role of surface roughness. J Chem Phys 2014;141:124701. doi: 10.1063/1.4895789

[14] M. Ciavarella (2018), A very simple estimate of adhesion of hard solids with rough surfaces based on a bearing areamodel, *Meccanica* Vol. 53, pp. 241–250. DOI 10.1007/s11012-017-0701-6

[15] J. A. Greenwood (2017), Reflections on and extensions of the Fuller and Tabor theory of rough surface adhesion, *Tribology Letters*, Vol. 65, Art. 159. doi: 10.1007/s11249-017-0938-1

[16] G. Carbone, E. Pierro and G. Recchia (2015), Loading-unloading hysteresis loop of randomly rough adhesive contacts, *Physical Review E*, Vol. 92, Art 062404. doi: 10.1103/PhysRevE.92.062404